Dalton Transactions

ROYAL SOCIETY OF CHEMISTRY

PAPER

View Article Online
View Journal | View Issue

Cite this: *Dalton Trans.*, 2025, **54**, 7449

Exploring the effect of Ru(II) arene complexes on cytotoxicity upon co-ligand variation and loading on amine-functionalized silica nanoparticles†

Srijita Pal, Pragti, Amardeep Kumar and Suman Mukhopadhyay *

To overcome the undesirable side effects and acquired resistance associated with platinum-based chemotherapeutics, scientists are searching for alternative strategies involving novel metal-based compounds with improved pharmacological properties. Ruthenium complexes have emerged as prospective candidates to combat side effects and improve the selectivity of anticancer agents. In this work, a benzimidazole-based chelating ligand, **HL** (4-(1*H*-naphth[2,3-*d*]imidazol-2-yl)-1,3-benzenediol) with O and N donor atoms, was synthesized and used for complexation with ruthenium to obtain three Ru(II) arene complexes represented by $[Ru(\eta^6\text{-}p\text{-cym})(L)Cl]$, $[Ru(\eta^6\text{-}p\text{-cym})(L)(PPh_3)]^+$ and $[Ru(\eta^6\text{-}p\text{-cym})(L)(PTA)]^+$ (where *p*-cym = *p*-cymene, PPh_3 = triphenylphosphine and PTA = 1,3,5-triaza-7-phosphaadamantane). The synthesized complexes were characterized using spectroscopic techniques. UV-Vis absorption spectroscopy and LC-MS were used to study the stability of the complexes in biological medium. Their lipophilicity was studied by calculating the partition coefficient in *n*-octanol and water. The complexes showed significant binding with biomolecules like albumin proteins and nucleic acids. All the complexes were found to be cytotoxic, with complex $[Ru(\eta^6\text{-}p\text{-cym})(L)PPh_3]PF_6$ exhibiting the highest anticancer activity. The mechanism of anticancer activity was attributed to the ability of the complexes to induce apoptosis and generate reactive oxygen species (ROS). The complexes also exhibited antimetastatic properties. Furthermore, complex $[Ru(\eta^6\text{-}p\text{-cym})(L)PPh_3]PF_6$ was loaded onto amine-functionalized mesoporous silica nanoparticles which led to an increase in its cytotoxic activity.

Received 24th December 2024,
Accepted 28th March 2025

DOI: 10.1039/d4dt03536d

rsc.li/dalton

1. Introduction

The discovery of cisplatin in the 1960s was a breakthrough in medicinal chemistry and cancer therapy. Cisplatin binds to N7 of guanine of DNA, causing inhibition of the cell division process and ultimately leading to apoptosis. Despite being effective against various cancers, it suffers from several side effects like nephrotoxicity, ototoxicity, and nausea, which occur because of lack of selectivity. The problems of toxicity and selectivity can be resolved using nanotechnology, but the problem of resistance acquired by cancer cells toward platinum-based drugs requires a novel solution. Thus, switching to alternative metal ions with different mechanistic pathways, greater target specificity and fewer side effects has become an urgent need.[1–3] Ruthenium(II) complexes because of their similar ligand exchange kinetics to platinum(II) complexes (similar to the cell division rate) and lesser toxicity seem to be promising candidates.[4] Also, since ruthenium can mimic iron in binding to biomolecules, it can be selectively transferred to cancer cells having overexpressed transferrin proteins on their membranes.[5] A few ruthenium(III) drugs, namely NAMI-A (imidazolium *trans*-[tetrachloro(dimethylsulfoxide)(1*H*-imidazole) ruthenium(III)]), KP1019 (indazolium *trans*-[tetrachlorobis(1*H*-indazole)ruthenium(III)]), and NKP-1339, the sodium salt of KP1019, have attracted a lot of attention as promising anticancer drugs but these drugs are not very stable and can undergo facile chemical transformations. These complexes are reduced to ruthenium(II) in the hypoxic acidic environment of tumor cells.[6,7]

RAPTA complexes, which stand for ruthenium arene PTA complexes, have gained significant attention over the last few years.[8] The hydrophobic arene ring facilitates the transportation of the drug molecule through the hydrophobic lipid bilayer of the cell membrane, and PTA (1,3,5-triaza-7-phosphaadamantane), a water-soluble ligand, enhances the aqueous solubility of the complex.[9] Also, by varying the other ligands, one can modulate the overall reactivity of the

Department of Chemistry, School of Basic Sciences, Indian Institute of Technology Indore, Simrol, Khandwa Road, Indore, 453552, India. E-mail: suman@iiti.ac.in; Tel: +91 731660 3328

† Electronic supplementary information (ESI) available. See DOI: https://doi.org/10.1039/d4dt03536d

complex. In addition to binding to DNA, these piano-stool complexes can also bind to serum proteins involved in transporting the drug molecules to the desired targets. They can also act as multitargeted drugs by targeting certain enzymes and peptides that are overexpressed in cancer cells.[10] The choice of ligand plays a major role in designing anticancer drugs. The dicarboxylate chelating ligand in carboplatin confers greater stability to the complex, resulting in fewer side effects than cisplatin.[11] Thus, the biological properties of ruthenium complexes can be modulated through appropriate choice of ligands.[12] The imine group in Schiff bases can form intermolecular hydrogen bonds with intracellular active components, resulting in various pharmacological applications. Ligands with extensive π-conjugation like phenanthroline, anthracene, naphthalene, and pyrene derivatives render fluorescent nature to the complexes, making them suitable for monitoring the probable mechanism of anticancer activity and cellular distribution.[13] Furthermore, benzimidazole derivatives, due to their similarity in structure to natural molecules, are known to possess several biological activities, such as antimicrobial, antifungal, and anticancer activities.[14] To increase the therapeutic performance of drugs, various nanocarrier-based delivery systems have been developed, which are known for targeted delivery and stimuli active nature. Mesoporous silica nanoparticles (MSNs), because of their several properties like tunable pore size, large surface area, biocompatibility, high stability, facile synthesis, and functionalization, prove to be an excellent candidate for delivering drugs.[15] Their ability to transport insoluble hydrophobic antitumor drugs and enable sustained release make them an efficient vehicle for drug delivery.[16] In particular, amine-functionalized MSNs (A-MSNs) are known to have higher loading capacity due to the formation of weak intermolecular forces between the amine group and the polar groups present in the drug molecule.[17] They are also known for improved cellular uptake of cationic ruthenium complexes arising due to the strong interaction between the positively charged surface of A-MSNs and the negatively charged phospholipids of the cell membrane.[18] The efficacy of anticancer platinum-based drugs is also known to improve upon using MSNs.[19]

This work involves the synthesis of a benzimidazole-based fluorescent ligand (HL) possessing inherent biological activity followed by its complexation with ruthenium to yield three ruthenium(II) arene complexes with *p*-cymene as the arene group. The objective of this work is to investigate the effect of co-ligands on anticancer activity and study the structure–activity relationship. Thus, the co-ligands have been varied between chloride (a good labile group that should facilitate the ligand exchange reactions as in cisplatin), triphenylphosphine (a hydrophobic group expected to facilitate the transportation of the ruthenium complex through the hydrophobic lipid bilayer of the cell membrane) and PTA (a water-soluble ligand which increases the overall water solubility of the complex). All the complexes were studied for their cytotoxicity on HeLa and DU145 cells, and the complex possessing the highest anticancer activity was further loaded on amine-functionalized MSNs (A-MSNs) to explore if its therapeutic potential gets enhanced upon incorporation into a drug delivery system.

2. Results and discussion

2.1 Synthesis and characterization

Three piano-stool Ru(II) arene complexes have been synthesized and characterized. The complexes have pseudo-octahedral geometry, with the arene moiety occupying three coordination sites and the bidentate chelating ligand **L** occupying two other coordination sites. N and O act as the donor sites for the chelating ligand. *p*-Cymene was chosen as the arene group because of its better structure–activity relationship (SAR) arising from its increased solubility.[20] The benzimidazole-based chelating ligand **HL** was chosen because of its inherent biological activity attributed to its structural similarity to the purine bases of DNA and the ability of its imine bond to form intermolecular H-bonds with intracellular components.[14] An additional phenyl ring was added to increase π-conjugation in the system rendering inherent fluorescence to the complex and a hydroxy group was introduced with the expectation of H-bonding interactions with the amine groups on A-MSNs.[13] **HL** was designed as a chelating ligand as chelating ligands are known to confer better chemical stability and thus lower toxicity.[11] The co-ligands were varied between chloride (Cl^-), PPh_3, and PTA. Cl^- was chosen because of its good leaving group nature which allows easy dissociation followed by coordination of the metal ion with biomolecules, thereby enhancing its structure–activity relationship (SAR).[20] PPh_3 was chosen because of its hydrophobic nature which is expected to facilitate the transportation of the drug through the cell membrane. In contrast, PTA, because of its water-soluble property, is expected to increase the aqueous solubility of the drug. The effect of global charge on the Ru(II) complex was also investigated by involving a neutral Ru(II) complex (**C1**) and two cationic Ru(II) complexes (**C2** and **C3**) in the study. For the cationic complexes, hexafluorophosphate was employed as a counterion, and NH_4PF_6 was utilized as the precursor. **C1** was synthesized by the reaction of the Ru *p*-cymene dimer and the ligand (**HL**). The chloride ligand was substituted with PPh_3 or PTA, followed by the addition of the necessary counter anions to obtain complexes **C2** and **C3**, respectively (Scheme 1). **MSN** was synthesized using the surfactant CTAB (cetyltrimethyl ammonium bromide) and the silica precursor TEOS (tetraethyl orthosilicate). APTES ((3-aminopropyl)triethoxysilane) was used to functionalize the surface of **MSN** with NH_2 groups and complex **C2** was loaded onto it. The synthetic procedures along with the reaction schemes are provided in the ESI.†

All the synthesized complexes were characterized using ESI-MS spectra. The ligand **HL** shows a base peak corresponding to $[H_2L]^+$, while for complex **C1**, the peak is obtained due to the $[RuL(p\text{-cym})]^+$ fragment after losing one chloride ion. Complexes **C2** and **C3** show peaks corresponding to the cationic complex part. The NMR data matched well with the predicted structures. The ^1H NMR peaks in the δ

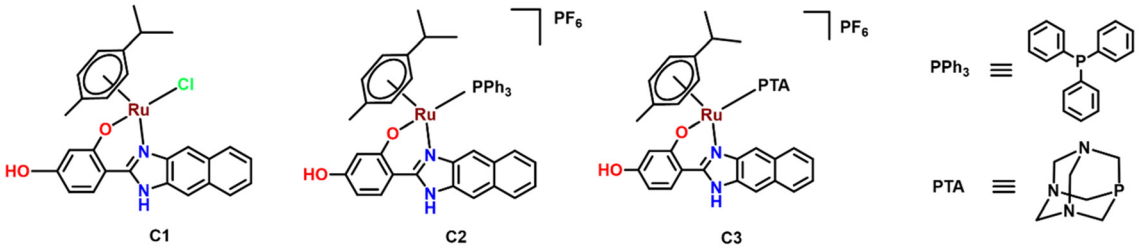

Scheme 1 Structures of the synthesized Ru(II) complexes **C1**, **C2**, **C3**.

5.25–6.05 ppm region correspond to the *p*-cymene aromatic protons, while the aromatic proton peaks of the ligand (**L**) appear at δ 8.27–6.45 ppm. The peaks at δ 2.8, 1.7–2.09, and 0.9–1.2 ppm are attributed to the methyl and isopropyl groups of the *p*-cymene ring. The highly deshielded broad peaks beyond 10 ppm correspond to OH and NH protons.[21] The PTA protons are observed in the region δ 4.73–4.26 ppm, and the peaks for the PPh_3 aromatic ring protons appear in the region δ 7.44–7.15 ppm (merging with the aromatic range of ligand **L**).[9]

The FTIR spectra of complexes **C1**, **C2**, and **C3**, and the ligand (Fig. S9†) exhibited a band at around 1600 cm^{-1} corresponding to the C=N functionality.[22] The bands for N–H and O–H stretching frequencies were found to overlap in the region of 3200–3460 cm^{-1}. The band at 1230–1240 cm^{-1} corresponds to the aromatic C–O stretching frequency. The presence of characteristic bands at 526 and 540 cm^{-1} in the IR spectra of **C2** and **C3** corresponds to the Ru–P stretching frequency, signifying successful complexation with ruthenium.[23] Bands at 831 and 821 cm^{-1} in case of complexes **C2** and **C3** arise due to the P–F stretching frequency of the counter anion.[24]

MSN, **A-MSN**, and drug-loaded **A-MSN** (**C2@A-MSNs**) were characterized using IR spectroscopy, FE-SEM, TGA, and BET. The FT-IR spectra of **MSN**, **A-MSN**, and **C2@A-MSNs** show bands at 1072 cm^{-1}, 794 cm^{-1}, and 456 cm^{-1} corresponding to the silanol groups (Si–O bond). The bare silanol groups on the surface of pristine **MSN** can be confirmed by bands at 3364 cm^{-1} and 1642 cm^{-1} corresponding to the deformation vibration of interlayer water and the OH stretching vibration of the silanol groups, respectively.[25] The amine functionalization of **MSN** was confirmed by the bending vibration mode of N–H which appeared at 1560 cm^{-1}.[18] The loading of complex **C2** on **A-MSNs** was confirmed by the imine band which appeared at 1604 cm^{-1}. The shift of the broad band corresponding to the O–H stretching frequency from 3300 cm^{-1} (free complex) to 3029 cm^{-1} (**C2@A-MSNs**) represents H-bonding interactions that may occur between the NH_2 groups of **A-MSNs** and the free OH group present in complex **C2** (Fig. S10†).[17]

The mesoporous nature of the **MSNs** and **A-MSN**s was characterized using N_2 adsorption–desorption analysis (Fig. S12†). The decrease in BET surface area from 752.617 m^2 g^{-1} to 68.326 m^2 g^{-1} and in pore diameter from 1.49202 nm to 1.32461 nm indicates the successful introduction of amine groups on the **MSN** surface. The surface area further decreased to 47.093 m^2 g^{-1} in **C2@A-MSN**s as **C2** was loaded onto the nanoparticles. This was further confirmed by the decrease in pore volume from 2.807×10^{-1} cc g^{-1} (MSNs) to 1.951×10^{-2} cc g^{-1} (A-MSNs) to 1.923×10^{-2} cc g^{-1} (**C2@A-MSNs**).[18] As observed from the TGA analysis, the drug-loaded system is thermally stable up to 200 °C as there is no significant weight loss except for the removal of water molecules and other solvents adsorbed on the surface (Fig. S11†).[26–29] The amorphous nature of the nanoparticles was confirmed by SEM images (Fig. S13†). The loading of complex **C2** onto **A-MSN**s causes the surface to appear rough. The powder X-ray diffraction pattern shows peaks corresponding to the hexagonal mesoporous pattern in **MSN** and **A-MSNs**.[17] The broad nature of the peaks also justifies the amorphous nature of the silica nanoparticles (Fig. S14†).

The absorption and emission spectra of all the complexes and the ligand were recorded in DMSO. In the UV-Vis spectra, two bands were observed for all the complexes and the ligand. The band at around 275–280 nm corresponded to the $\pi \rightarrow \pi^*$ transition, and the one at 340–360 nm corresponded to the $n \rightarrow \pi^*$ transition. An additional band was also observed only in the case of metal complexes in the range of 390–400 nm, which corresponds to the MLCT transition (Fig. S15a†).[30]

It is important to note that all the synthesized complexes and the ligand were found to be fluorescent. Their fluorescence spectra were recorded by exciting at a wavelength of 360 nm. Complex **C1** exhibited the highest fluorescence intensity, followed by complex **C2** and complex **C3** (Fig. S16†). The bands corresponding to the free **C2** complex were observed when the absorbance spectrum of **C2@A-MSNs** was recorded, indicating the successful loading of the drug onto amine-functionalized **MSNs**. The shift of the $n \rightarrow \pi^*$ transition to a lower wavelength in the case of **C2@A-MSNs** further confirmed the involvement of H-bonding interactions between **A-MSNs** and the polar groups of **C2** (Fig. S15b†).[31] SEM-EDX for the drug-loaded nanoparticles was also recorded, indicating the presence of Ru in **C2@A-MSNs**, which confirmed the successful loading of **C2** onto **A-MSNs** (Fig. S17a–c†).

2.2 Stability study

The stability of the complexes in biological medium was explored for the prospective application of the compounds as anticancer drugs. The complexes were dissolved in a 1% DMSO/PBS solution mixture, and the UV-Vis spectra were

recorded at 0, 6, 12, and 24 hours. The spectra showed no significant change or shift in band positions, indicating that the complexes are stable in the biological medium. Additionally, LC-MS data were recorded over a period of 48 hours and the main peak remained unaltered, confirming the integrity of the molecule in the biological medium (Fig. S19a–c†).

Since the tumor microenvironment is acidic in nature and the drug release study is performed at an acidic pH, it is crucial to check whether complex **C2** can maintain its integrity at a lower pH. Thus, the stability of complex **C2** at an acidic pH of 5.4 was monitored over 0, 24, 48, and 72 hours using absorption spectroscopy. No shift in the absorbance band indicated that the complex does not degrade in an acidic pH for up to 72 hours (Fig. S18†).

2.3 Lipophilicity study

Lipophilicity refers to the ability of a compound to pass through the lipid bilayer of the cell membrane and enter the cell. It is an important parameter regulating the cellular uptake of drugs. The lipophilicity of the synthesized and loaded complexes was determined from the partition coefficient $P_{O/W}$ in *n*-octanol and water by the shake-flask method. UV-Vis spectroscopy was used to determine the concentration of the complex in *n*-octanol (organic phase) and water (aqueous phase), and the partition coefficient was calculated. Complex **C2** and **C2@A-MSNs** with the triphenylphosphine group was found to have the highest partition coefficient values, making them the most lipophilic among all the tested complexes. This was probably due to the presence of the hydrophobic phenyl rings, which facilitate interaction in the non-polar medium.[21] Table S2† lists the partition coefficient values for the three complexes.

2.4 Protein binding study

2.4.1 Fluorometric titration. Serum albumin proteins are responsible for transporting drug molecules to the desired target through the enhanced permeability and retention (EPR) effect. This effect, which is a unique characteristic of tumors, allows for the accumulation of drugs in the tumor tissue.[32] Thus, it is important to know whether the synthesized complexes can bind with these proteins. Human serum albumin (HSA) and bovine serum albumin (BSA) which are inherently fluorescent in nature due to the presence of tryptophan amino acid residues were used to study the interaction between the metal complexes and protein. The environment of tryptophan is highly sensitive and presence of any external agents can alter the fluorescence intensity.[7] Fluorometric titration was performed where to a fixed concentration of BSA/HSA (10 μM) increasing amounts of metal complexes (0 μM–50 μM) were added and the change in fluorescence intensity was monitored. With increasing concentration of metal complexes, the fluorescence intensity at 335 nm corresponding to BSA/HSA decreased and a new peak emerged at around 445 nm when excited at 280 nm. The quenching of fluorescence intensity was attributed to the interaction of the complexes with the albumin protein while the increase in fluorescence intensity at a slightly higher wavelength was attributed to the inherent fluorescent nature of the complexes (Fig. 1 and S20†).

The binding parameters were calculated using the Stern–Volmer equation and the Scatchard equation (Fig. S21 and S22†). All the complexes exhibited significant interactions with proteins. The bimolecular quenching constants for all the complexes and the ligand are on the order of 10^{13}, indicating static quenching of fluorescence (Table S2†).[13] Complex **C1** shows a higher K_{SV} value because of the presence of a chloride ligand, which dissociates easily, leading to subsequent binding of other biomolecules to Ru.

2.5 Nucleic acid binding study

2.5.1 Absorption spectroscopy. Binding of complexes with nucleic acids like DNA and RNA can cause conformational changes, resulting in alterations of DNA/RNA-based processes.[33] Using UV-Vis spectroscopy, one can investigate the mode of interaction between the nucleic acids and the synthesized complexes. Hypochromism or a decrease in absorbance indicates intercalative interaction, whereas hyperchromism or an increase in absorbance signifies groove binding or other electrostatic interactions. When a fixed amount of the synthesized complexes or ligand was titrated with increasing amounts of nucleic acid, the absorbance decreased, indicating the intercalation of the planar aromatic rings between the DNA base pairs through π–π stacking (Fig. S23†).[33] Although nucleic acid binding studies were performed, it is noteworthy to mention here that these studies do not confirm that the complexes target the DNA or the nucleus. These studies were performed to get a perspective about the mode of interaction that these complexes can have if they can target the nucleic acids.

2.5.2 Emission spectroscopy. To further confirm the mode of interaction of the complexes with nucleic acids, a competitive fluorometric displacement assay was performed using ethidium bromide (EtBr). EtBr is a fluorescent tag that intercalates between the adjacent base pairs of nucleic acids. A decrease in fluorescence intensity was observed when an increasing amount of ruthenium complexes was added to a fixed concentration of the DNA–EtBr solution (Fig. S24†). The ruthenium complex displaces EtBr and gets intercalated between the base pairs, causing lowering of fluorescence intensity due to EtBr. This intercalation may lead to unwinding of the helical structure of DNA resulting in the inhibition of DNA replication process in cancer cells.[33] This assay was also performed with RNA, and a similar mode of binding was observed (Fig. S25†). The binding parameters were further calculated using the Stern–Volmer and Scatchard equation, which suggests significant binding of all the complexes with nucleic acids (Fig. S26, S27, and Table S4†).

2.6 Drug loading and pH-stimulated release study

Mesoporous silica nanoparticles (MSNs) because of their tunable properties have emerged as an efficient way of loading drugs and selectively delivering them to the desired target. Cytotoxicity of cisplatin was enhanced when it was loaded on

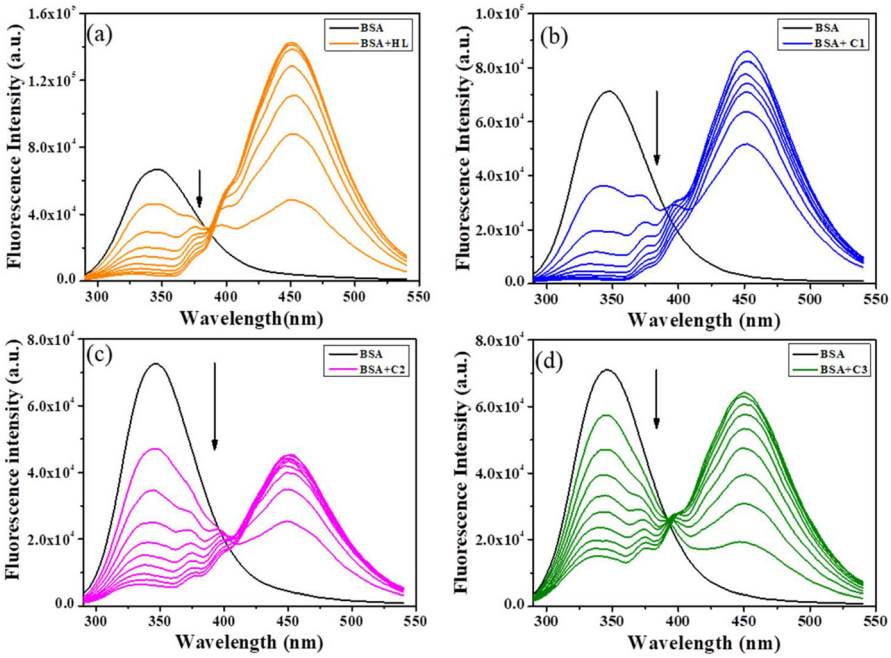

Fig. 1 Fluorometric titration spectra of BSA (10 μM) with (a) ligand (**HL**), (b) complex **C1**, (c) complex **C2**, and (d) complex **C3** at 298 K.

mesoporous silica materials (MCM-41 and SBA-15).[19] Doxorubicin when loaded on MSNs coated with polydopamine (PDA) and polyethylene glycol (PEG) exhibited higher cellular uptake and improved anticancer efficacy compared to the free drug.[34] The antibiotic drug rifampicin when encapsulated by MSNs resulted in better treatment efficiency than the free drug due to greater uptake by macrophages.[35] Since loading of drugs on MSNs significantly improves their efficiency compared to the free drug, the next target was to load the Ru(II) complex **C2** and see if there is any enhancement in anticancer activity. Determining the drug loading capacity of nanoparticles is crucial to study the drug activity and release. The loading capacity was found to be 40.4% (40 mg/100 mg) for **C2@A-MSNs** which was calculated using the weight % method (eqn (1)†).[36] Cancer cells have a hypoxic and acidic environment compared to normal cells. Thus, PBS buffers of acidic pH (5.4) and neutral pH (7.4) were used to investigate the selective release of drugs, specifically in cancer cells and normal cells. The drug release profile shows that in the case of neutral pH, after 4 hours, no detectable amount of the drug is released, and after 96 hours, only 30% of the drug is released. However, at acidic pH, a small amount of the drug is released in the initial hours, and 65% is released after 96 hours (Fig. 2). The greater amount of drug release in acidic pH may be attributed to the protonation of amine groups, causing the cleavage of H-bonding interactions between **A-MSNs** and the complex (Fig. 3).[18,26]

The integrity of the released drug **C2** was characterized by mass spectrometry. The appearance of a peak corresponding to the free complex **C2** in the mass spectrum after 96 hours at acidic pH confirmed the identity of the released complex (Fig. S28†).

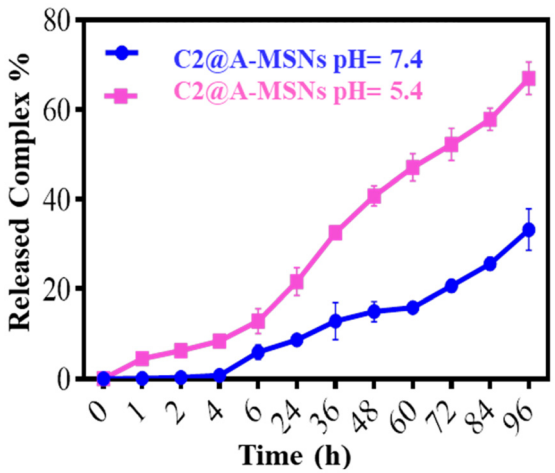

Fig. 2 Drug release profile of **C2@A-MSNs** at acidic and neutral pH.

2.7. Cell viability assay

An *in vitro* MTT assay was performed to determine whether the synthesized complexes were cytotoxic against cancer cells. MTT is a tetrazolium yellow-coloured salt that is reduced to formazan – a purple-coloured insoluble product in the presence of NADPH, an enzyme present only in live cells. Cancer cell lines HeLa and DU145 were treated with different concentrations (0–100 μM) of the synthesized Ru(II) complexes, and their IC_{50} values were calculated using the cell viability curve. All the complexes had potent cytotoxic activity against the above cell lines, and they were more responsive to HeLa cells (Fig. 4). Among the three complexes, complex **C2** was found to have the lowest IC_{50} value (17.78 μM in the case of HeLa and

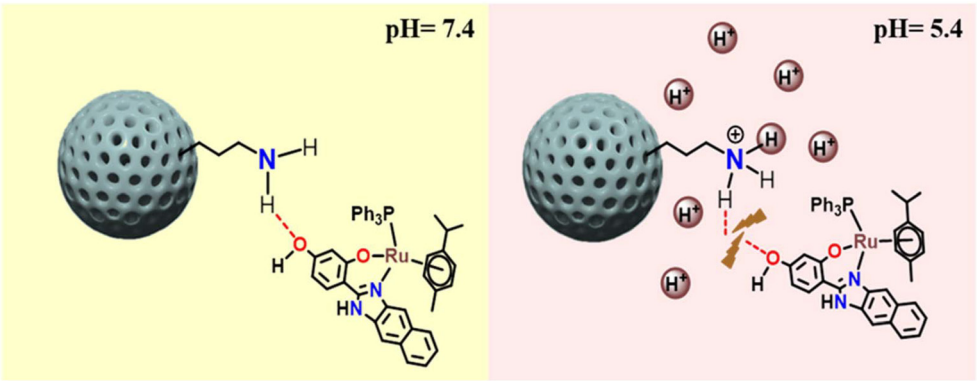

Fig. 3 Probable mechanism of drug release from **A-MSNs**.

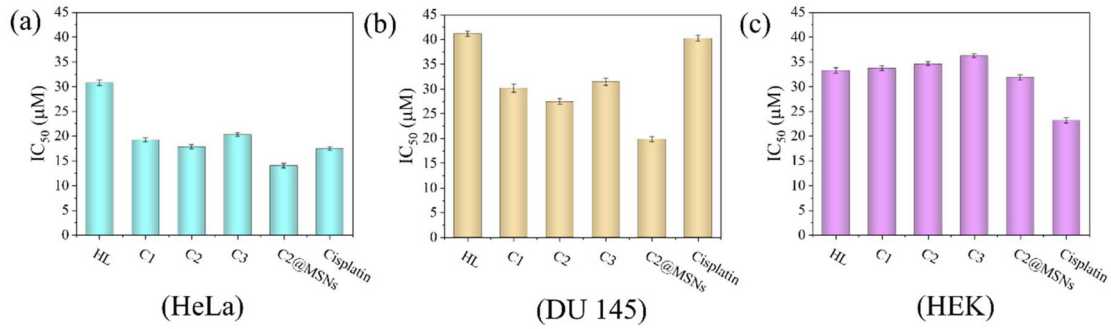

Fig. 4 Histogram representing the IC_{50} values (μM) of the ligand, three complexes and **C2@A-MSNs** for cancer cell lines (a) HeLa, (b) DU145 and (c) normal HEK 293 cells.

27.42 μM in the case of DU145) and, hence, the highest cytotoxicity which was attributed to the hydrophobic triphenylphosphine group which leads to enhanced hydrophobic interactions with biomolecules. These data are also in accordance with the results obtained from the lipophilicity study, which indicated the highest cellular uptake in case of complex **C2**. It is noteworthy to mention that all the complexes are active against cisplatin-resistant DU145 cells. The IC_{50} value further decreased upon loading complex **C2** on A-MSNs, indicating an enhancement in the cytotoxic profile. This was probably due to better cellular internalization occurring due to the interaction between negatively charged phospholipids and the positively charged surface of A-MSNs.[18] Also, the free ligand has a higher IC_{50} value than the ruthenium complexes indicating the advantage of the metal complexes over the free ligand. The complexes were also tested on normal cell lines HEK 293 and slight selectivity was observed for HeLa cell lines. Complex **C2** and **C2@A-MSNs** exhibited decent selectivity for the cancer cell lines over HEK 293 (Fig. 4 and S29†). The IC_{50} values for all the complexes and drug-loaded A-MSNs are listed in Table 1.

Table 1 IC_{50} values (μM) of the ligand, three complexes and **C2@A-MSNs** for cancer cell lines HeLa and DU145 and normal HEK 293 cells

IC_{50} values (in μM)			
Compounds	HeLa	DU145	HEK 293
Ligand HL	30.79 ± 0.56	41.13 ± 0.53	32.28 ± 0.45
Complex C1	19.21 ± 0.43	30.11 ± 0.83	33.73 ± 0.51
Complex C2	17.78 ± 0.48	27.42 ± 0.58	34.59 ± 0.59
Complex C3	20.26 ± 0.36	31.46 ± 0.74	36.21 ± 0.44
C2@A-MSNs	14.01 ± 0.43	19.83 ± 0.75	31.83 ± 0.39
Cisplatin	17.40 ± 0.38	40.22 ± 0.59	23.18 ± 0.28

2.8 Apoptosis study using a dual staining method

Since, **C2** and **C2@A_MSNs** were found to be the most potent among all the candidates, they were further studied for apoptosis, ROS generation and metastasis inhibition activity. The dual staining assay was performed using two DNA-binding dyes to study whether the complexes are potent of inducing apoptosis and to investigate the morphological changes associated with it. Acridine orange (AO) is a membrane-permeable dye capable of staining both viable and non-viable cells, and ethidium bromide (EtBr) is a membrane-impermeable dye, thereby capable of staining only non-viable cells with ruptured membranes. Upon binding to DNA, AO emits bright green fluorescence, while EtBr emits bright red fluorescence.[37] The confocal images show that **C2** and **C2@A-MSN**s are capable of inducing apoptosis. Morphological changes like ruptured cell

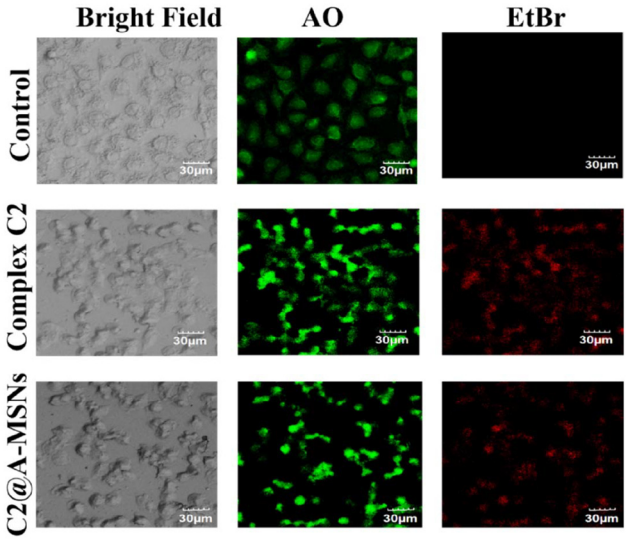

Fig. 5 Confocal images of HeLa cells stained with AO and EtBr after treatment with complex **C2** and **C2@A-MSNs**.

membranes and fragmented nuclei were observed, which are characteristic of apoptosis (Fig. 5). The apoptosis results for **C1** and **C3** are shown in Fig. S30.†

2.9 ROS generation: DCFH DA staining

The generation of reactive oxygen species (ROS) is an efficient way of killing cancer cells by producing oxidative stress inside the cells, which causes damage to intracellular substances. The generation of ROS in quantities greater than what can be scavenged by cellular enzymes like superoxide dismutase (SOD) causes oxidative damage to the cells. Additionally, because of the rapidly multiplying nature of cancer cells, they require a greater amount of oxygen than normal cells. Thus, converting oxygen into reactive oxygen species like superoxide anion, hydrogen peroxide, and $OH^{\bullet}$ can hamper cell division, thereby causing cell death.[38] Thus, the synthesized complexes were investigated for their ability to generate ROS using the DCFH-DA staining method. DCFH-DA (dichloro-dihydro-fluorescein diacetate) is a dye that, in the presence of ROS, gets oxidized to DCF, which emits green fluorescence.[39] Thus, it can be used for the detection of ROS. The microscope images clearly show green fluorescence only in the case of treated cells and not in the control, suggesting that **C2** and **C2@A-MSNs** can generate ROS, which are responsible for the green fluorescence (Fig. 6). Furthermore, from the fluorescence intensity graph (Fig. S31†), it is noticed that complex **C2** and **C2@A-MSNs** can generate ROS to a greater extent.

2.10 Metastasis inhibition

Metastasis refers to the spread of primary cancer cells to surrounding tissues and distant organs. The ability of cancer cells to migrate to non-malignant parts of the body and proliferate there makes it difficult to control the disease, making metastasis a dominant reason for mortality.[40] Thus, inhibiting the migration of malignant cells plays a major role in anticancer activity. To investigate the ability of the complexes to inhibit the cell migration process, a wound-healing assay was performed on HeLa cell lines. The cells were treated with the complexes at their IC_{50} values and the wound coverage was monitored for 24 hours. Compared to the control, where no drug was used, **C2** and **C2@A-MSNs** exhibited decreased wound coverage, indicating lesser cell migration to the scratched wound region (Fig. 7). Among the three free complexes, **C2** exhibited

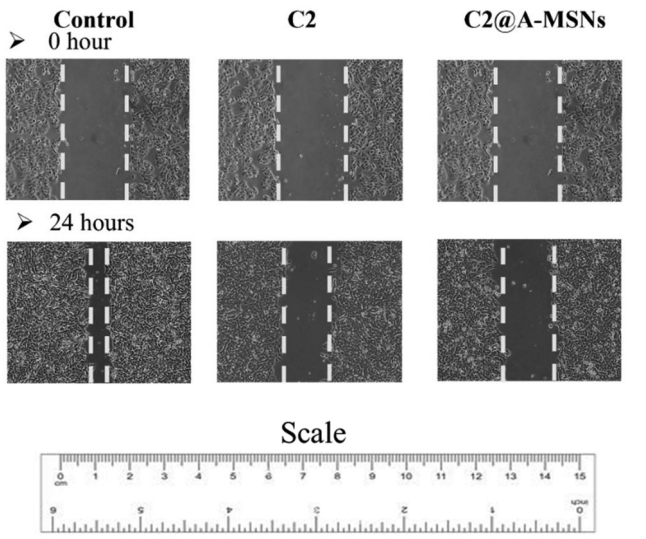

Fig. 7 Wound healing motility assay of HeLa untreated and treated cell with free complex **C2** and **C2@A-MSNs**. Images were taken at 0 and 24 h.

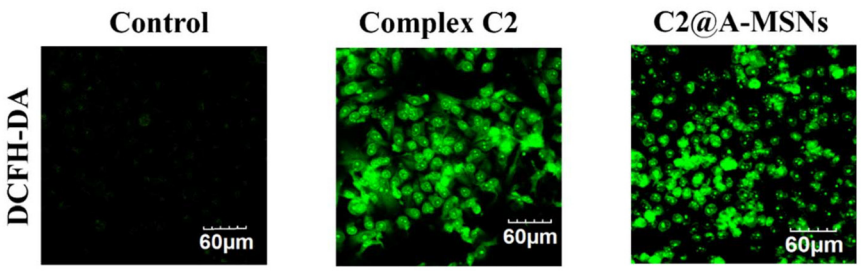

Fig. 6 ROS generation using the DCFH-DA assay for **C2** and **C2@A-MSNs**.

the maximum potential in inhibiting cell migration with a wound closure ratio of 35% and the antimetastatic property was further enhanced upon treatment with **C2@A-MSNs** (Fig. S32 and S33†).

3. Conclusion

Three ruthenium(II) arene complexes with *p*-cymene as the arene group and a bidentate benzimidazole-based chelating ligand with N and O as donor sites have been synthesized. The co-ligands have been varied between chloride, PPh_3 (triphenylphosphine) and PTA (1,3,5-triaza-7-phosphaadamantane). The complexes were characterized using several spectroscopic techniques like ESI-MS, IR, NMR and UV-Vis spectroscopy and their molecular formulas are found to be $[Ru(\eta^6\text{-}p\text{-cym})(L)Cl]$, $[Ru(\eta^6\text{-}p\text{-cym})(L)PPh_3]PF_6$, and $[Ru(\eta^6\text{-}p\text{-cym})(L)PTA]PF_6$. Both the ligand and the complexes were found to be fluorescent in nature. The complexes were studied for their lipophilic behaviour and complex **C2** was found to be the most lipophilic due to the increased hydrophobicity of the phenyl rings. All the complexes are stable in biological medium for up to 48 hours. Tryptophan quenching experiments suggested that the complexes significantly bind to albumin proteins like BSA and HSA. As is evident from absorption and emission spectroscopy, the complexes also show potent binding to CT-DNA and RNA and the mode of binding was found to be intercalation. However, this does not provide any evidence of DNA being the target molecule for exhibiting cytotoxicity. A cytotoxicity study was performed on HeLa and DU145 cells and all the complexes showed anticancer activity with better results on HeLa cells. Among all the three complexes, complex **C2** exhibited the lowest IC_{50} value and the highest anticancer activity due to the presence of the hydrophobic triphenylphosphine group which led to better interaction with the biomolecules as compared to chloride or PTA. The hydrophobic nature of the phenyl rings also increased the lipophilicity of the complex. The overall cationic charge of the complex also enhanced the solubility of the complex when compared to its neutral counterpart **C1**. Since complex **C2** was the most potent anticancer drug among the three complexes, it was loaded on amine-functionalized mesoporous silica nanoparticles to see whether these drug delivery nanocarriers can enhance its therapeutic performance. As observed from the cytotoxicity study, the anticancer activity was improved upon loading and their selectivity for cancer cells also increased. The enhancement in their therapeutic performance was attributed to the interactions between the negatively charged phospholipids and the positively charged surface of the nanoparticles which led to better cellular internalization. Complex **C2** and **C2@A-MSNs** were also capable of inducing apoptosis, generating ROS and exhibiting anti-metastatic activity on HeLa cell lines. In conclusion, the above synthesized complexes can act as potent anticancer agents and further studies can be conducted with *in vivo* tumor models.

Data availability

Synthetic procedures and experimental details of the *in vitro* biological study, detailed characterisation of the complexes and materials, and spectroscopic data can be found in the ESI.†

Conflicts of interest

There are no conflicts to declare.

Acknowledgements

The instrument facilities provided by SIC, IIT Indore, are gratefully acknowledged. The authors Prgati and Amardeep Kumar thank UGC and CSIR respectively for the fellowship. We gratefully acknowledge DST-FIST [Project No.- SR/FST/CSII/2017/22(C)] for providing a 500 MHz NMR facility.

References

1 S. Ghosh, *Bioorg. Chem.*, 2019, **88**, 102925.
2 R. Oun, Y. E. Moussa and N. J. Wheate, *Dalton Trans.*, 2018, **47**, 6645–6653.
3 S. H. van Rijt and P. J. Sadler, *Drug Discovery Today*, 2009, **14**, 1089–1097.
4 J. Reedijk, *Metallomics*, 2012, **4**, 628–632.
5 S. Y. Lee, C. Y. Kim and T.-G. Nam, *Drug Des., Dev. Ther.*, 2020, **14**, 5375–5392.
6 E. Alessio and L. Messori, *Molecules*, 2019, **24**, 1995.
7 Pragti, B. K. Kundu, C. Sonkar, R. Ganguly and S. Mukhopadhyay, *Polyhedron*, 2021, **207**, 115379.
8 R. Pettinari, F. Marchetti, F. Condello, C. Pettinari, G. Lupidi, R. Scopelliti, S. Mukhopadhyay, T. Riedel and P. J. Dyson, *Organometallics*, 2014, **33**, 3709–3715.
9 P. Mandal, N. Malviya, B. K. Kundu, S. S. Dhankhar, C. M. Nagaraja and S. Mukhopadhyay, *Appl. Organomet. Chem.*, 2018, **32**, e4179.
10 Pragti, B. K. Kundu and S. Mukhopadhyay, *Coord. Chem. Rev.*, 2021, **448**, 214169.
11 R. G. Kenny and C. J. Marmion, *Chem. Rev.*, 2019, **119**, 1058–1137.
12 H. A. Sahyon, A. A. El-Bindary, A. F. Shoair and A. A. Abdellatif, *J. Mol. Liq.*, 2018, **255**, 122–134.
13 Pragti, B. K. Kundu, S. N. Upadhyay, N. Sinha, R. Ganguly, I. Grabchev, S. Pakhira and S. Mukhopadhyay, *Dalton Trans.*, 2022, **51**, 3937–3953.
14 N. Shrivastava, M. J. Naim, M. J. Alam, F. Nawaz and S. Ahmed, *Arch. Pharm.*, 2017, **350**, e201700040.
15 Y. Li, G. Deng, X. Hu, C. Li, X. Wang, Q. Zhu, K. Zheng, W. Xiong and H. Wu, *Nanomedicine*, 2022, **17**, 1253–1279.
16 B. Siddiqui, A. ur. Rehman, I. Haq, A. A. Al-Dossary, A. Elaissari and N. Ahmed, *Int. J. Pharm.: X*, 2022, **4**, 100116.

17 R. Kotcherlakota, A. K. Barui, S. Prashar, M. Fajardo, D. Briones, A. Rodríguez-Diéguez, C. R. Patra and S. Gómez-Ruiz, *Biomater. Sci.*, 2016, **4**, 448–459.
18 M. M. Carmona, Q. P. Ho, J. Morand, A. García, E. Ortega, L. C. S. Erthal, E. R. Hernandez, M. D. Santana, J. Ruiz, M. V. Regí and Y. K. Gun'ko, *Inorg. Chem.*, 2020, **59**(14), 10275–10284.
19 Z. Tao, B. Toms, J. Goodisman and T. Asefa, *ACS Nano*, 2010, **4**, 789–794.
20 M. Martínez-Alonso, N. Busto, F. A. Jalón, B. R. Manzano, J. M. Leal, A. M. Rodríguez, B. García and G. Espino, *Inorg. Chem.*, 2014, **53**, 11274–11288.
21 P. Porwal, S. Nayek, S. Singh, A. Sonawane, I. Grabchev, R. Ganguly and S. Mukhopadhyay, *Dalton Trans.*, 2023, **52**, 7104–7118.
22 B. K. Kundu, Pragti, Reena, S. M. Mobin and S. Mukhopadhyay, *New J. Chem.*, 2019, **43**, 11483–11492.
23 J. G. Małecki and A. Maroń, *Transition Met. Chem.*, 2012, **37**, 727–734.
24 A. O. Adeloye, T. O. Olomola, A. I. Adebayo and P. A. Ajibade, *Int. J. Mol. Sci.*, 2012, **13**, 3511–3526.
25 P. Qin, Y. Yang, W. Li, J. Zhang, Q. Zhou and M. Lu, *Anal. Methods*, 2018, **11**, 105–112.
26 B. K. Kundu, Pragti, W. A. Carlton Ranjith, U. Shankar, R. R. Kannan, S. M. Mobin, A. Bandyopadhyay and S. Mukhopadhyay, *ACS Appl. Bio Mater.*, 2022, **5**, 190–204.
27 M. Almaghrabi, A. Alqurshi, S. A. Jadhav, F. Mazzacuva, A. Cilibrizzi, B. Raimi-Abraham and P. G. Royall, *Thermochim. Acta*, 2023, **730**, 179616.
28 H. Zhang, C. Li, J. Guo, L. Zang and J. Luo, *J. Nanomater.*, 2012, **2012**, 217412.
29 M. Mladenović, I. Morgan, N. Ilić, M. Saoud, M. V. Pergal, G. N. Kaluđerović and N. Ž. Knežević, *Pharmaceutics*, 2021, **13**, 460.
30 R. M. Ramadan, W. M. Elsheemy, N. S. Hassan and A. A. A. Aziz, *Appl. Organomet. Chem.*, 2018, **32**, e4180.
31 G. J. Brealey and M. Kasha, *J. Am. Chem. Soc.*, 1955, **77**, 4462–4468.
32 E. N. Hoogenboezem and C. L. Duvall, *Adv. Drug Delivery Rev.*, 2018, **130**, 73–89.
33 C. S. Devi, B. Thulasiram, S. Satyanarayana and P. Nagababu, *J. Fluoresc.*, 2017, **27**, 2119–2130.
34 Y. Duo, Y. Li, C. Chen, B. Liu, X. Wang, X. Zeng and H. Chen, *RSC Adv.*, 2017, **7**, 39641–39650.
35 S. Subramaniam, N. Thomas, H. Gustafsson, M. Jambhrunkar, S. P. Kidd and C. A. Prestidge, *Antibiotics*, 2019, **8**, 39.
36 G. Lv, L. Qiu, G. Liu, W. Wang, K. Li, X. Zhao and J. Lin, *Dalton Trans.*, 2016, **45**, 18147–18155.
37 K. Liu, P. Liu, R. Liu and X. Wu, *Med. Sci. Monit. Basic Res.*, 2015, **21**, 15–20.
38 H. Nakamura and K. Takada, *Cancer Sci.*, 2021, **112**, 3945–3952.
39 H. Kim and X. Xue, *J. Visualized Exp.*, 2020, **160**, DOI: **10.3791/60682**.
40 C. Sonkar, S. Sarkar and S. Mukhopadhyay, *RSC Med. Chem.*, 2022, **13**, 22–38.